nature geoscience

ARTICLES

https://doi.org/10.1038/s41561-019-0352-4

Stabilization of atmospheric nitrogen deposition in China over the past decade

Guirui Yu[1,2,11*], Yanlong Jia[3,11], Nianpeng He[1,2,4,11], Jianxing Zhu[1], Zhi Chen[1], Qiufeng Wang[1,2], Shilong Piao[5], Xuejun Liu[6,7], Honglin He[1,2], Xuebing Guo[1], Zhang Wen[6,7], Pan Li[8], Guoan Ding[9] and Keith Goulding[10]

Increasing atmospheric nitrogen deposition can influence food production, environmental quality and climate change from the regional to global scales. As the largest developing country, China is expected to experience a rapid increase in N deposition. However, the lack of information on dry N deposition limits our understanding of the historical trend of the total N deposition, as well as the main drivers of this trend. Here, we use extensive datasets that include both wet and dry N deposition to evaluate the spatiotemporal variation of N deposition and the changes of its components in China during 1980–2015. Three significant transitions in N deposition in China were observed. First, the total N deposition began to stabilize in 2001–2005, mostly due to a decline in wet NH_4^+ deposition. Subsequently, a shift to approximately equal wet and dry N deposition occurred in 2011–2015, accompanied by increasing dry deposition. Finally, the contribution of reduced N components in the deposition decreased due to increasing NO_3^- deposition. These transitions were jointly driven by changes in the socioeconomic structure in China and vigorous controls in N pollution. The three observed important transitions challenge the traditional views about the continuous increase in N deposition in China.

Rapid agricultural intensification, industrial and urban development, and increased fuel use in transportation and energy production have caused a dramatic increase in anthropogenic reactive nitrogen emissions over recent decades[1,2], which have been predicted to increase in China. Reactive N in the atmosphere is deposited via both dry and wet pathways involving reduced NH_x and oxidized NO_y species[1,3]. Despite their important and very different influences on the structure and function of terrestrial and marine ecosystems[4–7], few studies have quantified the separate components and N deposition pathways at the large (especially national) scale. Increased N deposition has profound consequences for natural and anthropogenic ecosystems. For example, N deposition provides a new source of fertilizer for plant growth but, conversely, can impact human health, modify biogeochemical cycles[3], change ecosystem structures and functions, and even result in species extinction[8–12]. N deposition may also influence ecosystem carbon cycles and, consequently, global climate change[11,13].

China is one of the three regions with the highest N deposition in the world[14]. It has increased by approximately 60% over the past 3 decades[15]. Previous studies have analysed the temporal and spatial variations of wet N deposition (F_{Wet}) and its components in China[16–18], but have not explored the temporal dynamics of dry deposition (F_{Dry}), mostly because of the difficulty in directly measuring and monitoring dry deposition[19,20]. The lack of information on dry deposition, the ratio of dry to wet N deposition ($R_{Dry/Wet}$) and the ratio of reduced to oxidized species (R_{NH_x/NO_y}) hinders our understanding of the spatial and temporal patterns of the flux of total N deposition (F_{Tot}).

Using a remote sensing model and nonlinear regression functions linking reactive N emissions and N deposition, we constructed herein a dataset for F_{Dry} across China for the period of 1980–2015. Together with the F_{Wet} data collected from 956 monitoring sites across China (2,376 site years of data) during 1980–2015, we explored the spatiotemporal patterns of the components of atmospheric N deposition (for example, F_{Tot}, F_{Dry}, F_{Wet}, $R_{Dry/Wet}$ and R_{NH_x/NO_y}) and their underlying mechanisms. Given the rapid socioeconomic changes in China and the parallel evolution of industries, combustion technologies and agricultural intensification, understanding the patterns of N deposition and the environmental and climate implications of N deposition is essential for environmental policy decisions in China—the largest developing country. However, such an improved understanding can also provide insights for other developing countries, and the global community generally, on managing and mitigating N cycles under the balance of socioeconomic development and controlling pollution.

Current status of atmospheric N deposition in China

The average F_{Tot} for China has been estimated as $20.4 \pm 2.6\,kgN\,ha^{-1}\,yr^{-1}$ in 2011–2015, where F_{Dry} and F_{Wet} were

[1]Key Laboratory of Ecosystem Network Observation and Modeling, Institute of Geographic Sciences and Natural Resources Research, Chinese Academy of Sciences, Beijing, China. [2]College of Resources and Environment, University of Chinese Academy of Sciences, Beijing, China. [3]Forestry College, Hebei Agricultural University, Baoding, China. [4]State Key Laboratory of Resources and Environmental Information System, Institute of Geographic Sciences and Natural Resources Research, Chinese Academy of Sciences, Beijing, China. [5]College of Urban and Environmental Sciences, Key Laboratory for Earth Surface Processes of the Ministry of Education, Peking University, Beijing, China. [6]Key Laboratory of Plant-Soil Interactions of MOE, College of Resources and Environmental Sciences, China Agricultural University, Beijing, China. [7]Beijing Key Laboratory of Farmland Soil Pollution Prevention and Remediation, College of Resources and Environmental Sciences, China Agricultural University, Beijing, China. [8]State Key Laboratory of Environmental Geochemistry, Institute of Geochemistry, Chinese Academy of Sciences, Guiyang, China. [9]Key Laboratory for Atmospheric Chemistry, Chinese Academy of Meteorological Sciences, Beijing, China. [10]Sustainable Agricultural Sciences Department, Rothamsted Research, Harpenden, UK. [11]These authors contributed equally: Guirui Yu, Yanlong Jia, Nianpeng He. *e-mail: yugr@igsnrr.ac.cn

Table 1 | Atmospheric dry, wet and total N deposition to China in 2011–2015

	Forms	Dry	Wet	Total
F_{Tot} (kgN ha^{-1} yr^{-1})[a]	NH_x	7.1 ± 0.6	5.9 ± 0.7	12.9 ± 1.3
	NO_y	3.2 ± 1.0	4.2 ± 0.5	7.5 ± 1.4
	$NH_x + NO_y$	10.3 ± 1.5	10.1 ± 1.2	20.4 ± 2.6
Total N deposition (TgN yr^{-1})[b]	NH_x	6.8 ± 0.6	5.7 ± 0.5	12.4 ± 1.2
	NO_y	3.1 ± 1.0	4.1 ± 0.2	7.2 ± 1.3
	$NH_x + NO_y$	9.9 ± 1.6	9.7 ± 1.3	19.6 ± 2.5
R_{NH_x/NO_y}	NH_x/NO_y	2.2 ± 0.2	1.4 ± 0.1	1.7 ± 0.1
$R_{Dry/Wet}$	Dry/Wet	-	-	1.0 ± 0.1

[a]The wet deposition of NH_x and NO_y was obtained by Kriging interpolation, while the dry deposition of NH_x and NO_y was calculated from remote sensing models (see Methods for details). The mean ± s.e. of each N deposition flux was calculated as the weighted average of 31 provinces in China, not including Hong Kong, Macao and Taiwan. The s.e. is the variation between the 31 provinces. [b]Total N deposition was calculated by multiplying the average fluxes by land area.

10.3 ± 1.5 and 10.1 ± 1.2 kgN ha^{-1} yr^{-1}, respectively (Table 1). Gaseous N and particulate N deposition contributed to 68.8 and 31.2% of F_{Dry}, respectively (Supplementary Table 1). Total N deposition to China was 19.6 ± 2.5 TgN yr^{-1}, which is very similar to its total anthropogenic N emission (about 20.8 TgN yr^{-1} in 2010[15]) and close to a modelling estimate for 2008–2012 (16.4 TgN yr^{-1})[21]. In comparison, F_{Tot} in the United States and Europe was approximately 6.01 and 10.02 kgN ha^{-1} yr^{-1}, respectively[22,23], and total N deposition in the United States and Europe was only 5.9 and 9.8 TgN yr^{-1}, respectively[23,24]. Unexpectedly, F_{Dry} was comparable to F_{Wet}, with $R_{Dry/Wet}$ approximately equal to 1 in China (Table 1), underlining the importance of F_{Dry} and its effects on terrestrial ecosystems. NH_x deposition dominated over NO_y in both F_{Dry} and F_{Wet}, with R_{NH_x/NO_y} values of 2.2 and 1.4, respectively.

The spatial patterns of NH_x and NO_y fluxes in dry and wet deposition in 2011–2015 were different (Fig. 1). The highest NH_x wet deposition ($F_{Wet(NH_x)}$) was measured in North, East and Central China. The spatial patterns of NO_y wet deposition ($F_{Wet(NO_y)}$) were similar to those of $F_{Wet(NH_x)}$, and NO_y deposition exceeded

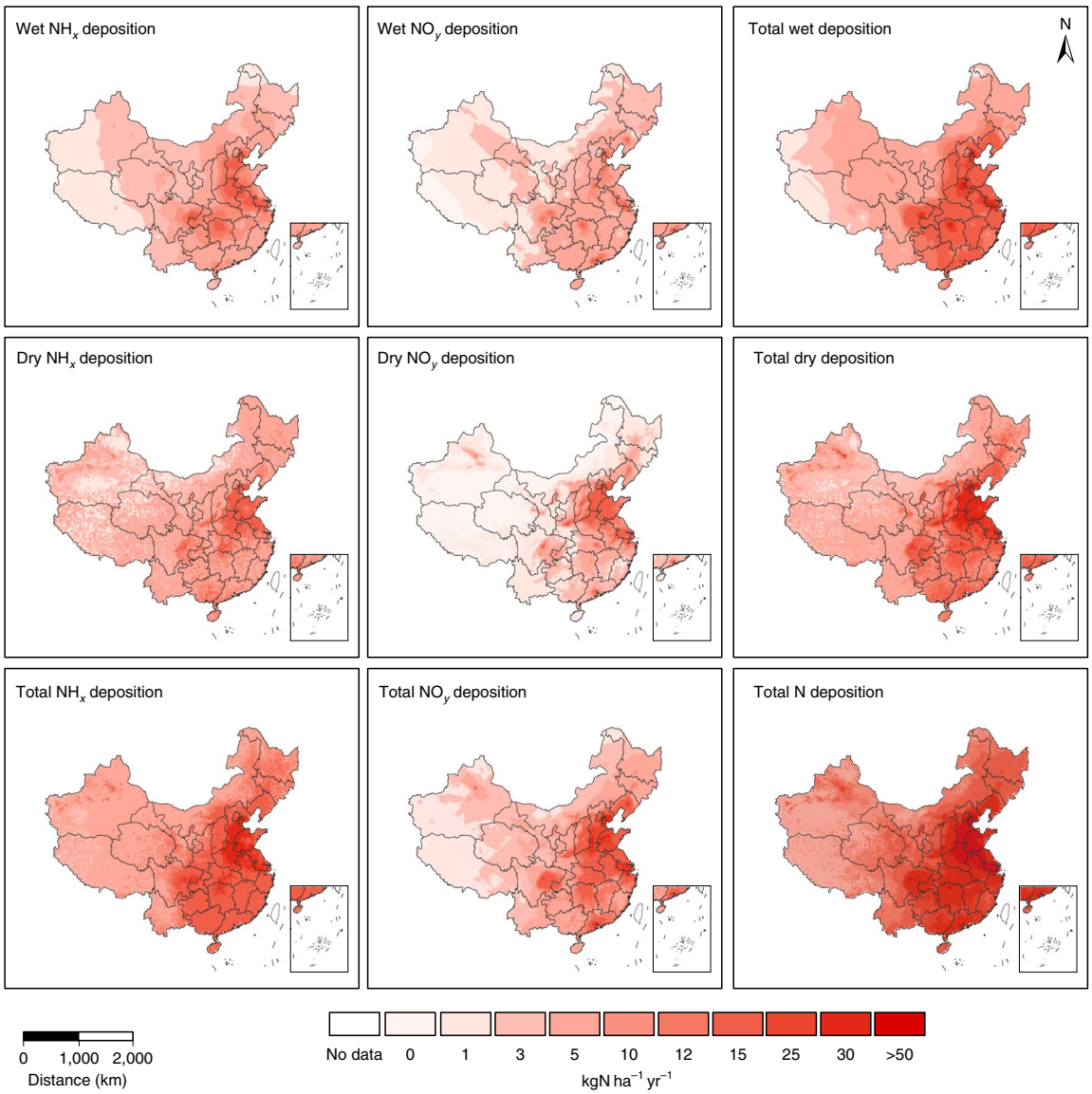

Fig. 1 | Spatial patterns of atmospheric N deposition over China in 2011–2015. The spatial patterns of wet deposition were obtained by Kriging interpolation, and those of dry deposition were obtained from remote sensing models.

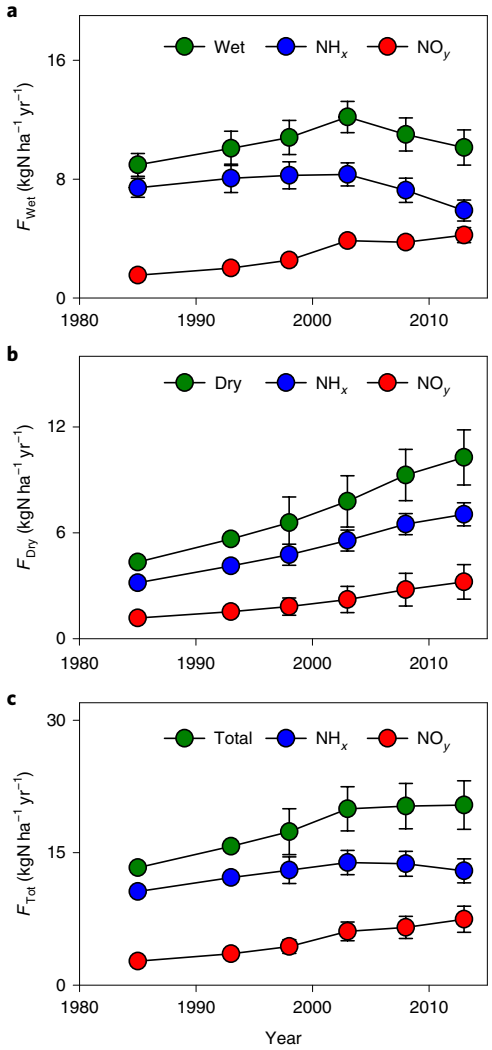

Fig. 2 | Temporal dynamics of wet, dry and total N deposition across China. a, Wet deposition ($F_{Wet(NH_x)}$ and $F_{Wet(NO_y)}$) was obtained by Kriging interpolation at intervals of five years during 1980–2015. **b**, Dry deposition was obtained from the remote sensing models ($F_{Dry(NH_x)}$ in 2008–2015 and $F_{Dry(NO_y)}$ in 1996–2015) and prediction functions ($F_{Dry(NH_x)}$ in 1980–2007 and $F_{Dry(NO_y)}$ in 1980–1996). **c**, Total deposition. Error bars indicate s.e. (the variation among the 31 provinces).

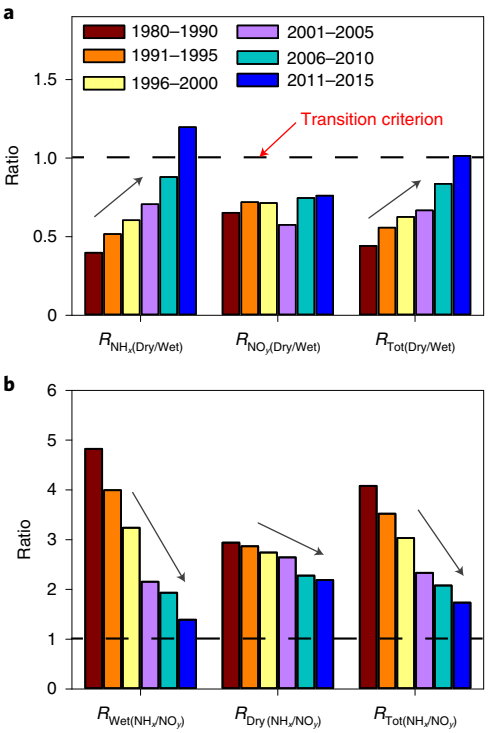

Fig. 3 | Temporal variations in $R_{Dry/Wet}$ and R_{NH_x/NO_y} in China. a, NH$_x$, NO$_y$ and total $R_{Dry/Wet}$. **b**, Wet, dry and total R_{NH_x/NO_y}. The dashed lines, as the equal contribution of dry and wet deposition, or NH$_x$ and NO$_y$ deposition, were considered as the transition criterion.

10 kgN ha^{-1} yr^{-1} over approximately 5.12% of the land area in China. Meanwhile, the highest NH$_x$ and NO$_y$ dry deposition was measured in North China. F_{Dry} exhibited a decreasing gradient from North China to other regions. The spatial pattern of F_{Tot} was similar to those of the NH$_x$ and NO$_y$ fluxes.

Gradual stabilization of total N deposition

The temporal evolution of F_{Tot} has changed from a rapid increase towards stability (Fig. 2c), with a similar trend occurring in most regions of China (Supplementary Fig. 1). F_{Wet} reached a peak in 2001–2005, then decreased by 17%, whereas F_{Dry} continued to increase (Fig. 2a,b), and similar annual dynamics of F_{Wet} and F_{Dry} are provided in Supplementary Fig. 2. The stability of F_{Tot} is unexpected and inconsistent with an earlier prediction of an ongoing increase in N deposition in China[15]. The cause is clear from a marked decline in $F_{Wet(NH_x)}$ (Fig. 2a). However, although $F_{Wet(NO_y)}$, $F_{Dry(NO_y)}$ and $F_{Dry(NH_x)}$ continued to increase during 2001–2010, $F_{Wet(NO_y)}$ and $F_{Dry(NO_y)}$ began to decrease after 2011 (Supplementary Fig. 2). Thus, the stabilization of F_{Tot} has been driven mostly by a gradual decline in $F_{Wet(NH_x)}$, but enhanced since 2011 by declines in both $F_{Wet(NO_y)}$ and $F_{Dry(NO_y)}$.

Measurements of F_{Wet} at 30 long-term wet N deposition monitoring sites, with >10 years of continuous data, offer robust evidence that the F_{Wet} deposition in China followed a quadratic relationship over time (Supplementary Fig. 3). At the site level, decreasing trends in F_{Wet} were observed at 18 of the 30 sites. In total, the peaked value of F_{Wet} by averaging these 30 sites was 21.3 kgN ha^{-1} yr^{-1} in 2006–2010. This decreased by 21% in 2011–2015. These results confirm the novel and important finding that the decreasing trend in F_{Wet} occurred in most regions across China.

A shift in wet and dry depositions

At a global scale, 40–80% of F_{NH_x} and 40–70% of F_{NO_y} are deposited via precipitation[14]. In China, atmospheric N deposition has shifted from being wet dominated to almost equal contributions of F_{Wet} and F_{Dry} (Fig. 3a). F_{Wet} accounted for 67% of F_{Tot} in 1980–1990, but decreased to 50% during 2011–2015 because F_{Dry} increased while F_{Wet} decreased.

From 1980 to 2015, $R_{Dry/Wet}$ increased on average by 0.02 yr^{-1} across China, with a general increase in all regions (Supplementary Fig. 4). In 2011–2015, N deposition in Northeast, North, East and Southwest China shifted from wet deposition dominating to approximately equal wet and dry deposition, with values of $R_{Dry/Wet}$ in the range 1.0–1.2. However, in Northwest, Central and South China, F_{Wet} remained dominant, with values of $R_{Dry/Wet}$ in the range 0.9–1.0, although $R_{Dry/Wet}$ still increased.

Decreased contribution of reduced (NH$_x$) components

R_{NH_x/NO_y} decreased significantly from 1980 to 2015, irrespective of changes in F_{Tot}, F_{Wet} and F_{Dry} (Fig. 3b). In particular, R_{NH_x/NO_y} in F_{Wet}

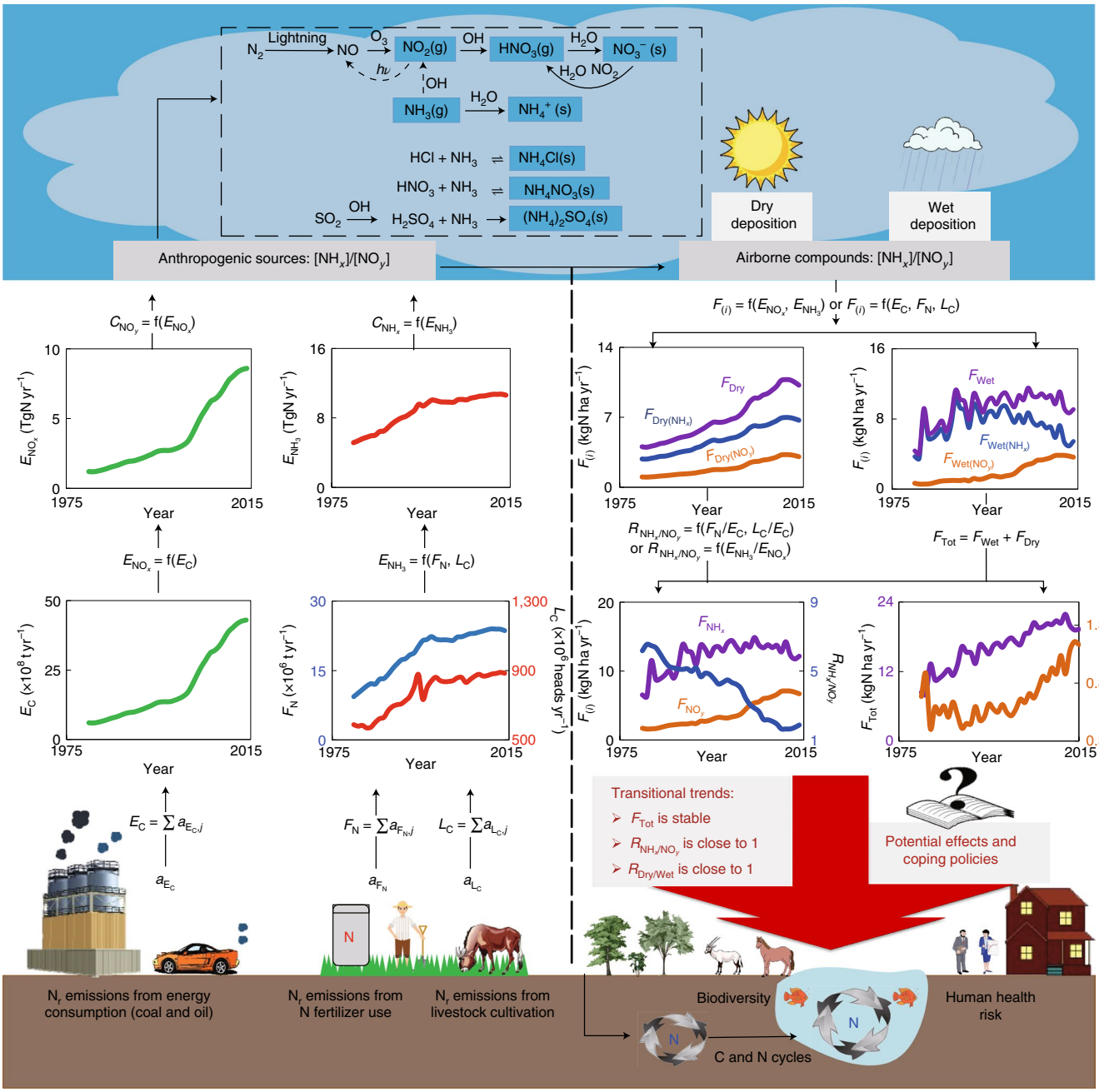

Fig. 4 | Mechanisms by which socioeconomic structures and environmental policies drove the transition of atmospheric N deposition in China. a_{E_C}, a_{F_N} and a_{L_C} denote energy consumption, N fertilizer use and livestock cultivation, respectively, by province. The variable '*C*' represents the concentration, *F* is the N deposition flux and *R* is the ratio. N_r represents reactive N.

decreased from 4.8 ± 0.3 to 1.4 ± 0.1. During 2011–2015, R_{NH_x/NO_y} values were much higher in Northwest and Southwest China, and lower in the remaining regions of China (Supplementary Fig. 4). In comparison, R_{NH_x/NO_y} in F_{Wet} increased from 0.7 in 1985 to 1.5 in 2012 in the United States[25]. Thus, R_{NH_x/NO_y} differed between developing and developed countries, which was probably the result of different phases of agriculture, industrialization and technological development.

The average R_{NH_x/NO_y} in the 7 Chinese regions significantly decreased by 0.086 yr^{-1} from 1996 to 2015, but at different rates in different regions (Supplementary Fig. 4). The maximum decline rates were observed in Northwest, Central and Southwest China, with an average rate of 0.11 yr^{-1}.

Contribution of socioeconomic structural changes

N fertilizer use (F_N) and livestock cultivation (L_C; that is, the number of large livestock units) are the main sources of anthropogenic NH_3 emissions via volatilization. Energy consumption (E_C, including industrial production and the combustion of coal, coke, oil, natural gas and other fuels) is the main source of NO_x[14,26]. From 1980–2015, F_N, L_C and E_C increased first, then stabilized in recent years because of the change in socioeconomic policies in China (Fig. 4), which together determined the spatiotemporal changes of atmospheric N deposition.

Rapid changes in economic development, industry infrastructure, energy consumption, and agricultural and environmental policies altered F_N, L_C and E_C, and their relative proportions (F_N/E_C or L_C/E_C), thereby influencing the emissions of reduced N and oxidized

N (E_{NH_3} and E_{NO_x}, respectively) and thus the ratio of reduced to oxidized components (E_{NH_3}/E_{NO_x}) (Fig. 4 and Supplementary Fig. 5). Structural equation modelling showed that F_N, L_C and E_C can together explain 96–99% of the spatiotemporal variation of reactive N emissions and 62–99% of the spatiotemporal variation of N deposition (Supplementary Fig. 6). Moreover, the variation of R_{NH_x/NO_y} (73–97%) and $R_{Wet/Dry}$ (43–84%) was explained well by the combined effects of mean annual precipitation (MAP), SO_2 emissions and reactive N emissions (Supplementary Fig. 7).

Since the reform and opening of China in the late 1970s, crop production and animal husbandry have intensified, resulting in a large increase in emissions of NH_3 and, consequently, a rapid increase in F_{NH_x} and F_{Tot} (Fig. 4). Since the mid-1990s, new agricultural policies and regulations have been implemented to restrict N emissions, such as two Chinese Ministry of Agriculture policies entitled 'Reducing the use of N fertilizer and improving the N use efficiency' and the 'Soil-testing and Fertilizer Recommendation Program'. These actions slowed the increases in F_N and L_C after the mid-1990s. In addition, the 'Zero Increase Action Plan' for national fertilizer use[27] was enacted in the 2010s, showing the strong stance of the Chinese government on fertilizer control and improving N use efficiency. Consequently, NH_3 emissions have been controlled and stabilized in recent years, leading to decreases in F_{NH_x} (Fig. 4).

Industrialization and urbanization in China in the 1980s were relatively slow. However, from the 2000s onwards, rapid urbanization, along with rapidly developing industry and increasing vehicle numbers, resulted in a rapid increase in E_C and subsequent direct increases in NO_x emissions. This resulted in a decrease in R_{NH_x/NO_y}, while a rapid increase was observed in F_{Tot}. Since 2010, new policies have been implemented for environmental protection, energy conservation and emission reductions, together with air pollution and vehicle-exhaust emission controls. The NO_x emission inventory verified that E_{NO_x} stabilized and even decreased slightly in recent years, resulting in the observed decreases in F_{NO_y} in both dry and wet deposition in the past five years (Supplementary Fig. 2b,e).

Industrialization and urbanization also increased SO_2 and NO_2 emissions and thus 'acid rain'. To mitigate the adverse effects of acid rain, a prevention plan for SO_2 emissions was implemented in two phases (1995 and 2008), which proved very effective (Supplementary Fig. 5b,e). SO_2 emissions in China declined after 2005 (Supplementary Fig. 8), which has influenced $R_{Dry/Wet}$ in N deposition over China. We found that SO_2 emissions were significantly negatively correlated with $R_{Tot(Dry/Wet)}$ and $R_{NH_x(Dry/Wet)}$, but showed no relationship with $R_{NO_y(Dry/Wet)}$ (Supplementary Fig. 9). The potential mechanism by which SO_2 emissions regulate $R_{Dry/Wet}$ can be explained by reactive preference and the non-reversible reaction between NH_3 and H_2SO_4 relative to HNO_3 or HCl (Supplementary Texts 1 and 2). Therefore, the reduction in SO_2 emissions has increased $R_{Dry/Wet}$ in N deposition, and especially that of NH_x deposition, supporting the results from the structural equation modelling (Supplementary Fig. 7).

Potential risks and challenges

Changes in N deposition and its composition in China can be characterized by a recent stabilization of total N deposition, accompanied by rapidly increasing dry deposition to a level approximately equal to wet deposition, and a decrease in R_{NH_x/NO_y}, caused by the socioeconomic structures and environmental policies of the Chinese government. The decrease of the NH_4^+ deposition was first observed in China. This was inconsistent with the earlier prediction of an ongoing increase[15], and differed from global trends[28]. Therefore, it is necessary to rethink the potential influence of N deposition on the terrestrial ecosystems in China. Most studies have assessed the impacts under the scenario of a continuous increase in N deposition[2,15], which now appears to be, at best, overestimated. Rather, models should consider a stable F_{Tot}, and the transitions in R_{NH_x/NO_y} and $R_{Dry/Wet}$, to assess the importance of shifts in $R_{Dry/Wet}$ and the chemical forms of N[6,29]. For example, dry N deposition can be absorbed by the plant canopy, whereas wet N deposition is mainly deposited onto the soil[4,30]. In addition, plant carbon sequestration could be increased by an increase in $R_{Dry/Wet}$, because canopy N uptake can enhance carbon sequestration by trees[6,31]. Plants can selectively absorb reduced and oxidized N forms, and species composition in plant communities could be altered with changes in R_{NH_x/NO_y} due to the preferential uptake of different N forms[7,32,33]. Also, the mechanisms by which NH_x and NO_y deposition influence soil acidification and greenhouse gas emissions differ[8,34,35]. The components of N deposition ($R_{Dry/Wet}$ and R_{NH_x/NO_y}) and how they vary over time need to be explicitly demonstrated.

Reducing N emissions while simultaneously sustaining economic development is a major challenge for all countries. Our results showed that, in China, programmes to control N fertilizer use have markedly decreased F_{NH_x}, providing a guide and a paradigm shift for other developing countries. The next step must be to further reduce NO_x emissions and achieve a continued decline in F_{NO_y}. One possible strategy for this is to change the energy structure. For example, the ongoing West–East Electricity Transmission Project would transmit electricity from hydroelectric generators in West China to East China, replacing coal-fired power production. Another possibility is to increase the chemical conversion of NO_x during fossil fuel combustion. China's Ministry of Ecology and Environment has taken several effective measures to modify heavy vehicle exhausts since 2013, promoting the application of selective catalytic reduction technology that can convert NO_x into N_2. These measures are expected to reduce NO_x emissions and decrease F_{NO_y} in China to some extent. The observed transitions in N deposition in China provide important insights into N cycle management and mitigation through rational socioeconomic policies that balance economic growth and pollution control in developing countries.

Online content

Any methods, additional references, Nature Research reporting summaries, source data, extended data, supplementary information, acknowledgements, peer review information; details of author contributions and competing interests; and statements of data and code availability are available at https://doi.org/10.1038/s41561-019-0352-4.

Received: 25 June 2018; Accepted: 14 March 2019;
Published online: 22 April 2019

References

1. Galloway, J. N. et al. Nitrogen cycles: past, present, and future. *Biogeochemistry* **70**, 153–226 (2004).
2. Liu, X. et al. Nitrogen deposition and its ecological impact in China: an overview. *Environ. Pollut.* **159**, 2251–2264 (2011).
3. Fowler, D. et al. The global nitrogen cycle in the twenty-first century. *Phil. Trans. R. Soc. B* **368**, 20130164 (2013).
4. Rennenberg, H. & Gessler, A. Consequences of N deposition to forest ecosystems—recent results and future research needs. *Water Air Soil Pollut.* **116**, 47–64 (1999).
5. Moran-Zuloaga, D., Dippold, M., Glaser, B. & Kuzyakov, Y. Organic nitrogen uptake by plants: reevaluation by position-specific labeling of amino acids. *Biogeochemistry* **125**, 359–374 (2015).
6. Nair, R. K., Perks, M. P., Weatherall, A., Baggs, E. M. & Mencuccini, M. Does canopy nitrogen uptake enhance carbon sequestration by trees? *Glob. Change Biol.* **22**, 875–888 (2016).
7. Song, M. H., Zheng, L. L., Suding, K. N., Yin, T. F. & Yu, F. H. Plasticity in nitrogen form uptake and preference in response to long-term nitrogen fertilization. *Plant Soil* **394**, 215–224 (2015).
8. Galloway, J. N. Acid deposition: perspectives in time and space. *Water Air Soil Pollut.* **85**, 15–24 (1995).
9. Stevens, C. J., Dise, N. B., Mountford, J. O. & Gowing, D. J. Impact of nitrogen deposition on the species richness of grasslands. *Science* **303**, 1876–1879 (2004).

10. Galloway, J. N. et al. Transformation of the nitrogen cycle: recent trends, questions, and potential solutions. *Science* **320**, 889–892 (2008).
11. Reay, D. S., Dentener, F., Smith, P., Grace, J. & Feely, R. A. Global nitrogen deposition and carbon sinks. *Nat. Geosci.* **1**, 430–437 (2008).
12. Templer, P. H., Pinder, R. W. & Goodale, C. L. Effects of nitrogen deposition on greenhouse-gas fluxes for forests and grasslands of North America. *Front. Ecol. Environ.* **10**, 547–553 (2012).
13. Van Groenigen, J. W. et al. Sequestering soil organic carbon: a nitrogen dilemma. *Environ. Sci. Technol.* **51**, 11503–11504 (2017).
14. Dentener, F. et al. Nitrogen and sulfur deposition on regional and global scales: a multimodel evaluation. *Glob. Biogeochem. Cy.* **20**, GB4003 (2006).
15. Liu, X. et al. Enhanced nitrogen deposition over China. *Nature* **494**, 459–462 (2013).
16. Lü, C. & Tian, H. Spatial and temporal patterns of nitrogen deposition in China: synthesis of observational data. *J. Geophys. Res.* **112**, D22S05 (2007).
17. Jia, Y. et al. Spatial and decadal variations in inorganic nitrogen wet deposition in China induced by human activity. *Sci. Rep.* **4**, 3763 (2014).
18. Zhu, J. et al. The composition, spatial patterns, and influencing factors of atmospheric wet nitrogen deposition in Chinese terrestrial ecosystems. *Sci. Total Environ.* **511**, 777–785 (2015).
19. Pan, Y. P., Wang, Y. S., Tang, G. Q. & Wu, D. Wet and dry deposition of atmospheric nitrogen at ten sites in Northern China. *Atmos. Chem. Phys.* **12**, 6515–6535 (2012).
20. Xu, W. et al. Quantifying atmospheric nitrogen deposition through a nationwide monitoring network across China. *Atmos. Chem. Phys.* **15**, 12345–12360 (2015).
21. Zhao, Y. et al. Atmospheric nitrogen deposition to China: a model analysis on nitrogen budget and critical load exceedance. *Atmos. Environ.* **153**, 32–40 (2017).
22. Li, Y. et al. Increasing importance of deposition of reduced nitrogen in the United States. *Proc. Natl Acad. Sci. USA* **113**, 5874–5879 (2016).
23. Holland, E. A., Braswell, B. H., Sulzman, J. & Lamarque, J. F. Nitrogen deposition onto the United states and western Europe: synthesis of observations and models. *Ecol. Appl.* **15**, 38–57 (2005).
24. Zhang, L. et al. Nitrogen deposition to the United States: distribution, sources, and processes. *Atmos. Chem. Phys.* **12**, 4539–4554 (2012).
25. Du, E. et al. Changes in wet nitrogen deposition in the United States between 1985 and 2012. *Environ. Res. Lett.* **9**, 095004 (2014).
26. Ianniello, A. et al. Chemical characteristics of inorganic ammonium salts in $PM_{2.5}$ in the atmosphere of Beijing (China). *Atmos. Chem. Phys.* **11**, 10803–10822 (2011).
27. Liu, X. et al. Evidence for a historic change occurring in China. *Environ. Sci. Tech.* **50**, 505–506 (2016).
28. Vet, R. et al. A global assessment of precipitation chemistry and deposition of sulfur, nitrogen, sea salt, base cations, organic acids, acidity and pH, and phosphorus. *Atmos. Environ.* **93**, 3–100 (2014).
29. Kuzyakov, Y. & Xu, X. Competition between roots and microorganisms for nitrogen: mechanisms and ecological relevance. *New Phytol.* **198**, 656–669 (2013).
30. Sievering, H., Tomaszewski, T. & Torizzo, J. Canopy uptake of atmospheric N deposition at a conifer forest: part I—canopy N budget, photosynthetic efficiency and net ecosystem exchange. *Tellus B* **59**, 483–492 (2007).
31. Thomas, R. Q., Canham, C. D., Weathers, K. C. & Goodale, C. L. Increased tree carbon storage in response to nitrogen deposition in the US. *Nat. Geosci.* **3**, 13–17 (2010).
32. McKane, R. B. et al. Resource-based niches provide a basis for plant species diversity and dominance in arctic tundra. *Nature* **415**, 68–71 (2002).
33. Ashton, I. W., Miller, A. E., Bowman, W. D. & Suding, K. N. Niche complementarity due to plasticity in resource use: plant partitioning of chemical N forms. *Ecology* **91**, 3252–3260 (2010).
34. Gavrichkova, O. & Kuzyakov, Y. Ammonium versus nitrate nutrition of *Zea mays* and *Lupinus albus*: effect on root-derived CO_2 efflux. *Soil Biol. Biochem.* **40**, 2835–2842 (2008).
35. Li, X. et al. The contrasting effects of deposited NH_4^+ and NO_3^- on soil CO_2, CH_4 and N_2O fluxes in a subtropical plantation, southern China. *Ecol. Eng.* **85**, 317–327 (2015).

Acknowledgements

This work was supported by the National Key Research and Development Program of China (2016YFA0600104 and 2017YFA0604803), Chinese Academy of Sciences Priority Research Program (XDA19020302), National Natural Science Foundation of China (31872690, 31700377, 31570471 and 31290221), programme of the Youth Innovation Research Team Project (LENOM2016Q0005), National Postdoctoral Program for Innovative Talents (BX20180300) and Newton Fund through the BBSRC project of the China Virtual Joint Centre for Improved Nitrogen Agronomy (BB/N013468/1).

Author contributions

G.Y. designed the research. Y.J., N.H., J.Z., H.H., X.G. and P.L. conducted the research (collected the datasets and analysed the data). G.Y., Y.J., N.H., S.P., X.L., K.G. and J.Z. wrote the manuscript. Q.W., W.Z., G.D. and Z.C. commented on the manuscript.

Competing interests

The authors declare no competing interests.

Additional information

Supplementary information is available for this paper at https://doi.org/10.1038/s41561-019-0352-4.

Reprints and permissions information is available at www.nature.com/reprints.

Correspondence and requests for materials should be addressed to G.Y.

Publisher's note: Springer Nature remains neutral with regard to jurisdictional claims in published maps and institutional affiliations.

Methods

Data sources for wet N deposition. Wet N deposition data were obtained from four sources: published peer review articles for 1980–2015; our own monitoring data from 41 sites of the Chinese Ecosystem Research Network for 2013–2015; monitoring data from 43 sites from the Nationwide Nitrogen Deposition Monitoring Network (NNDMN), established by China Agricultural University, for 2010–2014; and monitoring data from 81 stations of the National Acid Deposition Monitoring Network, established by the China Meteorological Administration, for 1992–1993. The criteria for data selection were as follows: measurement of N concentrations or deposition fluxes in rainfall, including NH_4^+ and NO_3^- (dissolved inorganic nitrogen being the sum of NH_4^+ and NO_3^-); a sampling frequency of every precipitation event, daily or weekly; and a sampling period covering more than one year. The datasets included the name of the monitoring site, location, monitoring period, monitoring method, ecosystem type, annual precipitation, and the concentration and deposition of NH_4^+, NO_3^- and dissolved inorganic nitrogen.

If the data were the average N concentration in rainfall, the corresponding N deposition was calculated based on the N concentration and annual precipitation. If the data were bulk deposition, we converted bulk N deposition to wet N deposition (F_{Wet}). When analysing studies that measured N deposition using two sampling methods (bulk N deposition versus F_{Wet}), for NH_4^+ and NO_3^- deposition, we found a significant linear relationship between F_{Wet} deposition and bulk deposition (slope range: 0.67–0.77, R^2 range: 0.91–0.94; all $P < 0.0001$). Therefore, we transformed bulk N deposition into F_{Wet} using a coefficient of 0.70. After rigorous data screening and quality control, we obtained a total of 2,376 site years (956 stations) of F_{Wet} during 1980–2015 (Supplementary Fig. 10).

To study the spatiotemporal pattern of wet N deposition, we divided the datasets into six subsets of five-year intervals. The number of monitoring sites in the 1980s was limited; hence, we treated the data from 1980–1990 as one subset. Therefore, the 6 datasets contained 126, 152, 135, 208, 260 and 171 sites for the periods of 1980–1990, 1991–1995, 1996–2000, 2001–2005, 2006–2010 and 2011–2015, respectively. The monitoring sites covered the main terrestrial ecosystems in China, including forest, grassland, cropland, shrub land, desert, wetland and urban ecosystems.

Determination of the spatial patterns and temporal evolution of F_{Wet}. It should be noted that different scaling-up methods, from site to region, resulted in different estimates of N deposition in China, because of higher spatial heterogeneity and unbalanced economic development in different regions[15–17]. We analysed wet N deposition in China using three scaling methods, namely Kriging interpolation, arithmetic averaging and weighting based on land area (Supplementary Text 3 and Supplementary Fig. 11), and compared the data with those of Europe and the United States (Supplementary Table 2). Ultimately, we chose Kriging interpolation to evaluate the spatial pattern of N deposition.

We constructed national-scale F_{Wet} maps using Kriging interpolation with ArcGIS version 10.0 software. Kriging is a method of providing unbiased estimates of variables in limited regions with minimum variance based on variogram theory and structural analysis, and has been widely used in the spatial evaluation of N deposition in different regions[16,23]. The inputs were site year data of wet N deposition ($F_{Wet(NH_x)}$ and $F_{Wet(NO_y)}$) with longitude and latitude for the periods of 1980–1990, 1991–1995, 1996–2000, 2001–2005, 2006–2010 and 2011–2015. The specific process of interpolation included an exploration of data analysis, testing and transformation of the normal distribution of data, and determination of the optimum variogram model and its parameters. The details of the interpolation method have been published previously[17]. The spatial patterns of $F_{Wet(NH_x)}$ and $F_{Wet(NO_y)}$ were generated for the years of 1980–1990, 1991–1995, 1996–2000, 2001–2005, 2006–2010 and 2011–2015, while those of F_{Wet} were obtained based on the sum of $F_{Wet(NH_x)}$ and $F_{Wet(NO_y)}$ in the corresponding periods.

To verify the accuracy of the interpolation, we validated the results using independent data from the period 2011–2015. The validation data were derived from the NNDMN networks of 43 monitoring stations[20]. The R values for the correlation of $F_{Wet(NH_x)}$, $F_{Wet(NO_y)}$ and F_{Wet} were 0.78, 0.63 and 0.78, respectively. The root mean square error was lower than 5.0 for all comparisons (Supplementary Fig. 12). These results show that Kriging interpolation can depict the spatial and temporal patterns of wet N deposition.

Sources of remote sensing data. NO_2 column data. NO_2 vertical tropospheric columns were derived from the Tropospheric Emission Monitoring Internet Service (www.temis.nl). The NO_2 column data were obtained from three satellites: the Global Ozone Monitoring Experiment (GOME), Scanning Imaging Absorption Spectrometer for Atmospheric Chartography (SCIAMACHY) and Ozone Monitoring Instrument (OMI)[36,37]. Supplementary Table 3 presents the NO_2 column data from the satellites. We downloaded the global monthly product of the NO_2 columns between January 1996 and December 2015 as an ESRI grid and calculated the mean annual NO_2 column.

We used the NO_2 column data from the 3 satellites to cover a 20-year period, because no other long-term data from the satellites were available. Differences in overpass time between the sensors, such as OMI aboard Aura with an overpass time of 13:30 and SCIAMACHY aboard Envisat with an overpass time of 10:00, caused NO_2 columns to be observed by satellites differently[38]. To determine the differences between the annual NO_2 column data originating from different satellites, we compared data from grids observed simultaneously by two satellites during overlapping time periods, such as GOME (1996–2003) versus SCIAMACHY (2002–2012) (choosing data from 2002), and SCIAMACHY (2002–2012) versus OMI (2004–present) (choosing data from 2005) (Supplementary Fig. 13). The results showed that the observational data from GOME were approximately 10% higher than those obtained from SCIAMACHY, and SCIAMACHY data were approximately 30% higher than those from OMI. Using Supplementary Equations (1) and (2), the GOME and SCIAMACHY data were normalized to the OMI data (Supplementary Fig. 14). The data from GOME covered the period 1996–2002, the data from SCIAMACHY covered the period 2003–2004, and the data from OMI spanned 2005–2015.

NH_3 column data. NH_3 columns were derived from the Infrared Atmospheric Sounding Interferometer—a Fourier transform infrared spectrometer that was launched aboard the polar sun-synchronous MetOp platform in October 2006[39,40]. It crosses the equator at 09:30 and 21:30 local solar time, can offer near-global coverage twice per day, and has a square footprint of 12 km × 12 km at nadir and an elliptical footprint of 20 km × 39 km off nadir, depending on the satellite viewing angle[41].

We obtained the daily NH_3 column data from the ESPRI Data Centre, from January 2008 to December 2015, including day and nighttime data. The availability of measurements was determined using the method of Liu et al.[42]. The observations had to meet 3 criteria: the cloud coverage was <25%; the relative error was <100%; and the absolute error was $<5 \times 10^{15}$ molecules cm^{-2}. After eliminating invalid values, the remaining negative values were replaced by the mean of ambient 0.05° data. We calculated the annual NH_3 column mean by averaging the daily NH_3 columns within 0.25° latitude × 0.25° longitude.

Determination of the spatial patterns and temporal evolution of dry N deposition. In our previous research, we developed remote sensing models to estimate global F_{Dry} using NO_2 satellite and ground measurements[43]. NNDMN uses the same F_{Dry} monitoring methods at 43 sites across China[20], providing a useful approach for directly estimating F_{Dry} with empirical remote sensing models.

Because NO_2 is a source of gaseous HNO_3 and particulate NO_3^- (ref. [26]), ground concentrations of NO_2, HNO_3 and NO_3^- can be estimated using NO_2 satellite measurements[43]. We explain herein the methods used to evaluate the spatial patterns of F_{Dry} at an annual scale in China using NO_2 F_{Dry} as an example. First, the NO_2 ground concentrations from the 43 monitoring sites and corresponding annual NO_2 columns were paired. Second, an appropriate model (linear or nonlinear) was selected to establish an empirical model, and the intercept was set to zero to decrease the overestimation of low NO_2 deposition values. Third, leave-one-out cross-validation was used to validate the models. In this analysis, each monitoring site was individually removed, and the estimated value from the models of the remaining sites was compared with the original value. Fourth, the spatial pattern of the NO_2 ground concentrations was evaluated using the established empirical models. Fifth, the spatial pattern of the NO_2 deposition fluxes was estimated based on the NO_2 ground concentrations multiplied by the corresponding deposition velocity. The spatial patterns of NH_3 and NH_4^+ were estimated with the same method using the NH_3 column and ground measurements from the NNDMN.

The empirical models for estimating the ground concentrations of NO_2, HNO_3, NO_3^-, NH_3 and NH_4^+ were established (Supplementary equations (3)–(7)) and the results of cross-validation are as expected (Supplementary Fig. 15). GlobCover 2009[44] was used to determine land use, and the velocities of different N components for various land-use types were derived from the literature (Supplementary Table 4).

Based on the aforementioned methods and the long time series of NO_2 and NH_3 column data, we estimated the F_{Dry} of NO_2, HNO_3 and NO_3^- in 1996–2015, as well as the F_{Dry} of NH_3 and NH_4^+ in 2008–2015. Because the NH_3 columns in 2015 showed a sharp increase, possibly due to artificial causes from the updated input data[42], the spatial patterns of NH_3 and NH_4^+ in 2015 were replaced with those from 2014.

Analysis of spatiotemporal variability of N deposition. The main sources of NH_3 and NO_x emissions are N fertilizer, livestock cultivation and fossil fuel combustion. NH_3 and NO_x in the atmosphere ultimately deposit to land and water surfaces after a series of chemical conversions and physical transport. Therefore, N emissions and their driving factors can affect the spatiotemporal variability of N deposition. We first analysed the single effect of N emission and its driving factors, including F_N, L_C and E_C, on N deposition by regression analyses (Supplementary Tables 5 and 6). Then, we analysed the effect of driving factors on N emissions (Supplementary Table 7). Finally, we looked at the effect of N emissions on N deposition (Supplementary Table 8). Due to a lack of NH_3 column data in 1980–2007 and NO_2 column data in 1980–1995, annual dry NH_x and NO_y deposition fluxes in these periods were predicted from E_{NH_3} and E_{NO_x} (Supplementary Table 8). The temporal and spatial changes in the MAP exerted a weak impact on the amounts and components of N deposition (Supplementary Tables 5 and 6).

We determined the prediction functions of wet and dry N deposition as driving parameters (Supplementary Table 9). The statistical relationships were used to describe the temporal and spatial variations in $F_{Wet(i)}$ and $F_{Dry(i)}$ as equations (1) and (2), respectively:

$$F_{Wet(i)} = F_{max} \times [1 - \exp(a \times (b \times F_N + c \times L_C + d \times E_C))] + e \quad (1)$$

$$F_{Dry(i)} = a \times (b \times F_N + c \times L_C + d \times E_C) + e \quad (2)$$

where the F_{max} values for $F_{Wet(NH_x)}$, $F_{Wet(NO_y)}$ and F_{Wet} in the temporal variation of $F_{Wet(i)}$ were 10, 5 and 15 kgN ha^{-1} yr^{-1}, respectively, and the F_{max} values for $F_{Wet(NH_x)}$, $F_{Wet(NO_y)}$ and F_{Wet} for the spatial variation of $F_{Wet(i)}$ were 15, 10 and 25 kgN ha^{-1} yr^{-1}, respectively. As with the contribution of precipitation to gross primary productivity in the 'Miami model'[45], the relationship between wet N deposition and N emissions also showed a saturation curve. Therefore, we determined F_{wet} as equation (1), and the determination of F_{max} was based on the maximum value of wet N species in their temporal or spatial variation. In the equations, a is a constant coefficient, b, c and d represent the emission factors of F_N, L_C and E_C, respectively, and e represents the natural source of N deposition ($\leq$1 kgN ha^{-1} yr^{-1} for NH_x or NO_y in dry or wet deposition; $\leq$2 kgN ha^{-1} yr^{-1} for total dry or wet deposition). For the temporal scale, the units of F_N, L_C and E_C were 10^4 tN yr^{-1}, 10^4 heads yr^{-1} and 10^4 t coal yr^{-1}, respectively. At the provincial scale, the units of F_N, L_C and E_C were tN km^{-2}, heads km^{-2} and t coal km^{-2}, respectively.

Considering the combined effects of F_N, L_C and E_C, a general model was developed, as in equation (3), to describe the temporal and spatial variations in R_{NH_x/NO_y} in N deposition:

$$R_{(NH_x/NO_y)} = a \times [(b \times F_N + c \times L_C)/(d \times E_C)] + e \quad (3)$$

Sources of statistical data. The annual precipitation for the period 1980–2013 was obtained from the China Meteorological Administration, comprising 756 weather stations across China. The MAP in each province was calculated based on the annual precipitation from the weather stations in each specific province. The data on the annual amounts of F_N, L_C, poultry production, industrial production and E_C between 1980 and 2015 were derived from the National Bureau of Statistics of China (http://data.stats.gov.cn/), China Statistical Yearbook and China Energy Statistical Yearbook.

N and SO_2 emissions in China. Annual NH_3, NO_x and SO_2 emissions in China between 1980 and 2015 were obtained from the literature and the China Environment Yearbook (Supplementary Table 10). Because fewer emissions data were available in 2010–2015 than before 2010, we processed the data between 2011 and 2015 differently. If the emissions data were available until 2011, but not until 2015, we approximated data to 2015 according to the trend of emissions using an optimal fitting model. Finally, we obtained the averaged N and S emissions for each specific year (Supplementary Fig. 8). The provincial NH_3, NO_x and SO_2 emissions in China in 2012 were derived from the Model of Multi-resolution Emission Inventory for China established by Tsinghua University[46–49], which was downloaded from http://www.meicmodel.org/index.html.

Data analysis. All data were analysed with SPSS version 13.0 statistical software. The correlation analyses relating F_N, L_C, E_C, precipitation, and spatial and temporal variations in N deposition used linear or nonlinear regression models according to the values of the correlation coefficients (r) and P. We used multiple regression analysis to establish the equations for exploring the spatial and temporal variations in N deposition. The structural equation model was used to explore the predicators of the spatiotemporal patterns of wet and dry N deposition and their ratios. All figures were drawn using SigmaPlot version 12.0 software. The spatial pattern figures for N deposition were plotted with ArcGIS 10.0 software.

Uncertainty analysis. The estimation methods for N deposition represented one of the sources of uncertainty, such as the empirical remote model for F_{Dry} and the interpolation method for wet deposition. The validation showed that the regression coefficients were greater than 0.6 for both F_{Dry} and F_{Wet} (Supplementary Figs. 12 and 15). However, the limited number of observation sites for F_{Dry}, and the uneven distribution of observation sites for F_{Wet}, require better data in the future for higher precision. Also, the effects of the changes in precipitation on atmospheric N deposition were difficult to quantify. Models could be used to study the effects of changing rainfall intensity or rainy days under global climate change scenarios. Finally, organic N deposition was not considered here because of the limited availability of data, complexity of its components, and transformation processes. Some studies have reported that dissolved organic N deposition at a global scale accounts for 25–30% of F_{Wet}[50], suggesting that dissolved organic N deposition requires much more work in the future.

Data availability

The data that support the findings of this study are available from the corresponding author upon request. The data sources for the NO_2 column, NH_3 column, social statistics, and NH_3, NO_x and SO_2 emissions can be found in the Methods.

Code availability

The code used to generate and process NH_3 column data can be accessed on request to Y.J.

References

36. Boersma, K., Eskes, H. & Brinksma, E. Error analysis for tropospheric NO_2 retrieval from space. *J. Geophys. Res.* **109**, D04311 (2004).
37. Boersma, K. et al. An improved retrieval of tropospheric NO_2 columns from the Ozone Monitoring Instrument. *Atmos. Meas. Tech.* **4**, 1905–1928 (2011).
38. Boersma, K. et al. Intercomparison of SCIAMACHY and OMI tropospheric NO_2 columns: observing the diurnal evolution of chemistry and emissions from space. *J. Geophys. Res.* **113**, D16S26 (2008).
39. Hilton, F. et al. Hyperspectral Earth observation from IASI: five years of accomplishments. *Bull. Am. Meteorol. Soc.* **93**, 347–370 (2012).
40. Van Damme, M. et al. Global distributions, time series and error characterization of atmospheric ammonia (NH_3) from IASI satellite observations. *Atmos. Chem. Phys.* **14**, 2905–2922 (2014).
41. Clarisse, L., Clerbaux, C., Dentener, F., Hurtmans, D. & Coheur, P. F. Global ammonia distribution derived from infrared satellite observations. *Nat. Geosci.* **2**, 479–483 (2009).
42. Liu, L. et al. Temporal characteristics of atmospheric ammonia and nitrogen dioxide over China based on emission data, satellite observations and atmospheric transport modeling since 1980. *Atmos. Chem. Phys.* **15**, 9365–9378 (2017).
43. Jia, Y. et al. Global inorganic nitrogen dry deposition inferred from ground- and space-based measurements. *Sci. Rep.* **6**, 19810 (2016).
44. Arino, O., Ramos, J., Kalogirou, V., Defourny, P. & Achard, F. In *Proc. ESA Living Planet Symposium* (2010).
45. Lieth, H. Primary production: terrestrial ecosystems. *Hum. Ecol.* **1**, 303–332 (1973).
46. Zhang, Q. et al. Asian emissions in 2006 for the NASA INTEX-B mission. *Atmos. Chem. Phys.* **9**, 5131–5153 (2009).
47. Li, M. et al. Mapping Asian anthropogenic emissions of non-methane volatile organic compounds to multiple chemical mechanisms. *Atmos. Chem. Phys.* **14**, 5617–5638 (2014).
48. Zheng, B. et al. High-resolution mapping of vehicle emissions in China in 2008. *Atmos. Chem. Phys.* **14**, 9787–9805 (2014).
49. Liu, F. et al. High-resolution inventory of technologies, activities, and emissions of coal-fired power plants in China from 1990 to 2010. *Atmos. Chem. Phys.* **15**, 13299–13317 (2015).
50. Cornell, S. E. et al. Organic nitrogen deposition on land and coastal environments: a review of methods and data. *Atmos. Environ.* **37**, 2173–2191 (2003)